Supplementary Information

Biomimetic Reusable Microfluidic Reactors with Physically-Immobilized RuBisCO for Glucose Precursor Production

Yujiao Zhu[a, b], *Qingming Chen*[c], *Chi Chung Tsoi*[a], *Xiaowen Huang*[d], *Abdel El Abed*[e], *Kangning Ren**[b], *Shao-Yuan Leu*[f] *and Xuming Zhang**[a]

[a] Department of Applied Physics, The Hong Kong Polytechnic University, Hong Kong, 999077, P. R. China

[b] Department of Chemistry, Hong Kong Baptist University, Hong Kong, 999077, P. R. China

[c] School of Microelectronics Science and Technology, Sun Yat-sen University, Zhuhai, 519082, P. R. China

[d] State Key Laboratory of Biobased Material and Green Papermaking; Shandong Provincial Key Laboratory of Microbial Engineering, Department of Bioengineering, Qilu University of Technology (Shandong Academy of Sciences), Jinan, 250353, P. R. China

[e] Laboratoire Lumière Matière et Interfaces (LuMIn), Institut d'Alembert, ENS Paris Saclay, CentraleSupélec, CNRS, Université Paris-Saclay, 4 avenue des Sciences, 91190 Gif-sur-Yvette, France

[f] Department of Civil and Environmental Engineering, Hong Kong Polytechnic University, Hong Kong, 999077, P. R. China

* Corresponding author. E-mails: apzhang@polyu.edu.hk; kangningren@hkbu.edu.hk

S1. Soft photolithography

Briefly, a 4″ silicon wafer was firstly cleaned by acetone, ethanol, and deionized water (DIW), followed by drying in an oven to remove any contamination. Then, the SU-8 was spin-coated to a thickness of 40 μm (at 500 rpm for 15 s followed by 2500 rpm for 60 s) on the cleaned wafer and then soft-baked at 65 ^{o}C for 5 min and another baking step at 95 ^{o}C for 15 min. The soft-baked SU-8 was then exposed to UV light for 45 s (with exposure energy of 180 mJ/cm^2), followed by a post-baking process at 65 ^{o}C for 5 min and at 95 ^{o}C for 15 min (as shown in Step 1 of Figure S1). Afterward, the SU-8 was developed in SU-8 developer for 3 min and then washed with isopropyl alcohol (IPA) for 10 seconds, followed by air dry using compressed nitrogen. Finally, the mold was hard baked at 150 ^{o}C for 5 min. The SU-8 mold was ready for further use (Step 2). Next, the PDMS compound that was formed by mixing PDMS and its curing agent at a weight ratio of 10:1 was poured into the SU-8 mold and put on a hot plate at 85 ^{o}C for 30 min (Step 3).

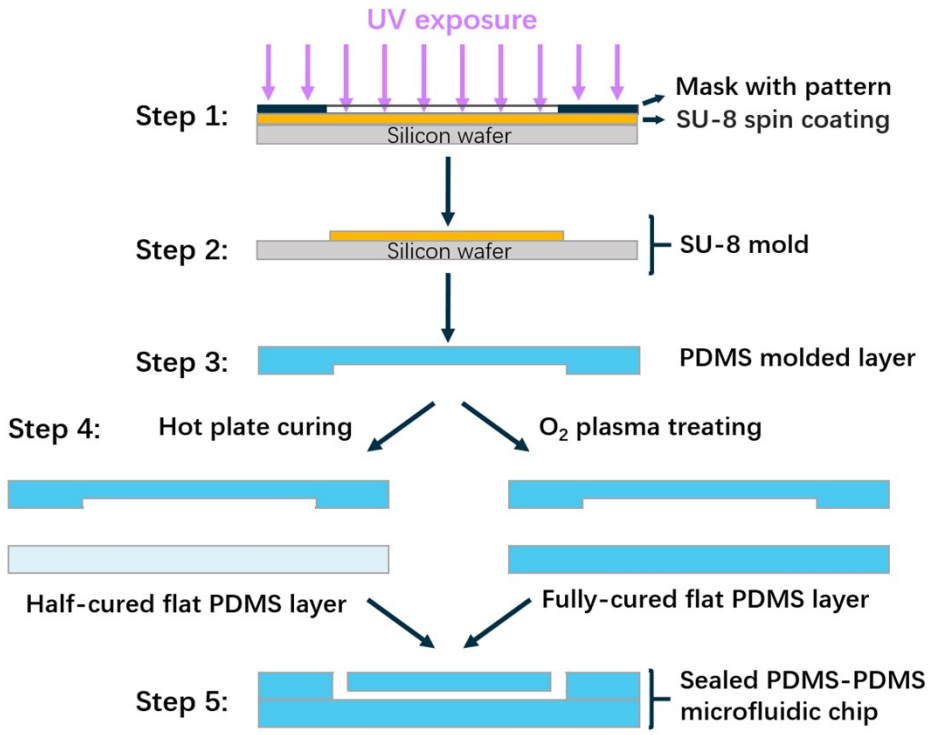

Figure S1. Process flow of the fabrication of PMRs by the soft photolithography technique. The fabrication procedures include soft photolithography, PDMS molded and flat layers fabrication, and microfluidic chip sealing.

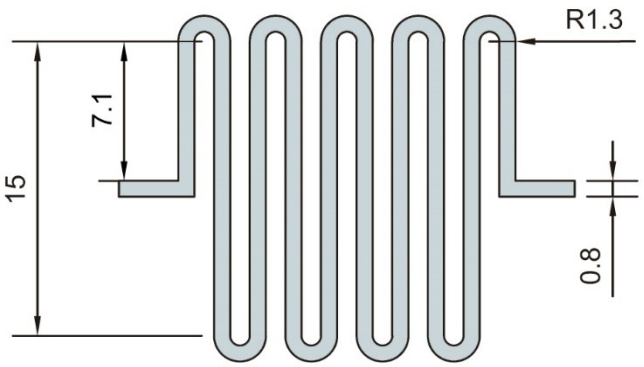

Figure S2. Detailed dimensions of the microchannels as shown by the gray-blue area. The unit is millimeter. The height of the microchannel is 40 μm.

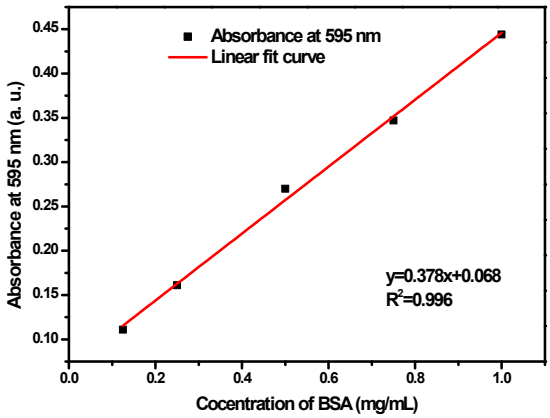

Figure S3. Calibration of protein amount determined from BSA solutions by the Bradford method. Protein amount was qualified using the Quick Start Bradford Protein Assay kit (Bio-Rad Pacific Limited.), which were determined by measuring the absorbance at the wavelength of 595 nm using a UV-Visible spectrometer (UV-2450, Shimadzu). BSA solutions (0.125-1 mg mL^{-1}) were selected as standards to plot the calibration curve.[1, 2]

S2. Amplification method for RuBisCO activity assay

For the immobilized RuBisCO activity assay, reactant mixture (66 mM HCO_3^- and 0.5 mM RuBP in the reaction buffer) was passed through the RIMRs and the production solution (containing RuBisCO, RuBP, HCO_3^- and 3-PGA in the reaction buffer) was collected from the outlet of the reactors for further assay. 20 μL of the production solutions were added with 80 μL of assay mixture (the final concentrations were 5 unit mL^{-1} PGK, 0.5 unit mL^{-1} GAPDH, 0.5 unit mL^{-1} TPI, 0.5 unit mL^{-1} G3PDH, 1 unit mL^{-1} G3POX, 1000 unit mL^{-1} catalase, 0.5 mM ATP, 2 mM NADH, 1.5 mM $MgCl_2$ and 100 mM Tricine/KOH pH 8.0). The reaction was immediately and continuously monitored by measuring the absorbance change at 340 nm by a UV-Visible spectrometer. During the reaction, the product 3-PGA was first converted to dihydroxyacetone-phosphate (DAP) with PGK, GAPDH, ATP and NADH. Catalase was also added here to prevent the inhibition of GAPDH. Then, DAP was transformed into the cycle of mutual conversion with glycerol-3 phosphate (G3P). It could be monitored as the cumulative oxidation of NADH, whose amount was much larger than the original amount of 3-PGA, therefore providing strong amplification of signal for 3-PGA monitoring (Figure S4a). The signal of production solutions could be converted to the specific amount of 3-PGA by using a standard curve generated by adding different amounts of standard 3-PGA into the assay mixture as shown by the dark solid squares in Figure S4b.

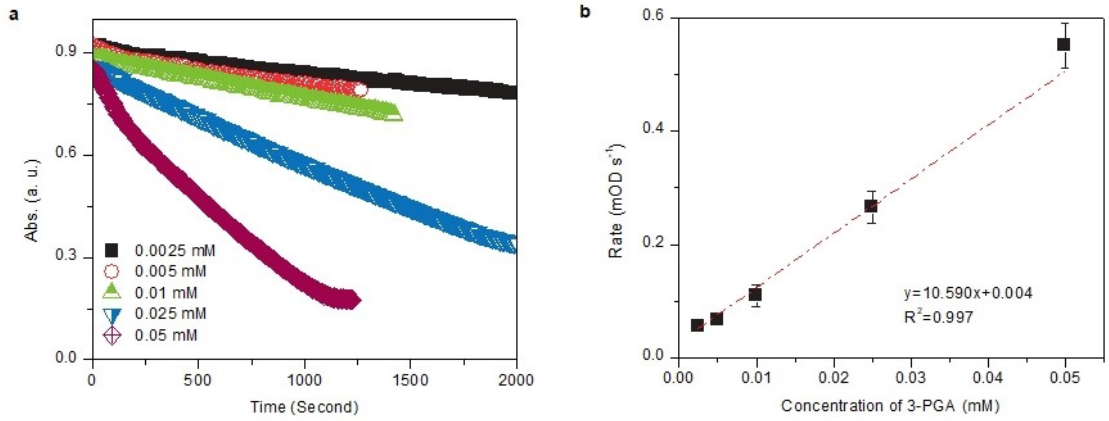

Figure S4. Calibration of standard 3-PGA amount by UV-Visible spectrometry. (a) Decrease of the absorbance at 340 nm as a function of the time for different concentrations (from 0.0025 to 0.05 M) of 3-PGA dissolved in the reaction buffer. (b) Calibration line of 3-PGA in the reaction buffer by the amplification signal assay with using the UV-Vis spectrometer. Error bars represent the standard deviations from three independent experiments.[1]

S3. Reaction time determination in RI-PMRs

The reaction time t_r is regarded as the residence time of the reaction mixture flowing through the RI-PMRs, which is calculated by the equation of

$$t_r = V_r/Q \quad \text{(S1)}$$

where V_r is the volume of the RI-PMRs and Q is the flow rate of the injected RuBP solution controlled by the syringe pump. In this work, the volume of RI-PMR is 7 μL, the corresponding reaction time is 1 min, 5 min, 7 min, 10 min for the flow rates of 7 μL min^{-1}, 1.4 μL min^{-1}, 1 μL min^{-1}, 0.7 μL min^{-1}, respectively.

S4. Confirmation of RuBisCO immobilization by fluorescence experiments

RuBisCO was tagged with fluorescein isothiocyanate isomer I (FITC) to confirm the successful immobilization. FITC-tagged RuBisCO (RuBisCO-FITC) solution was firstly injected into the microchannels. After incubation of 4 h at room temperature, the microchannels were washed by the reaction buffer. As shown in Figure S5, the fluorescence intensity difference (noted as Δ(FI)) between the microchannel and the microchannel wall was obvious when the RuBisCO-FITC solutions were filled into the microchannels. After the thoroughly rinsing by the PBS buffer, Δ(FI) decreased but not drops to zero. The non-zero Δ(FI) after the rinse proved that a portion of RuBisCO was well retained on the microchannel surface, therefore confirming the successfully immobilization of RuBisCO inside the microfluidic reactor via the physical adsorption.

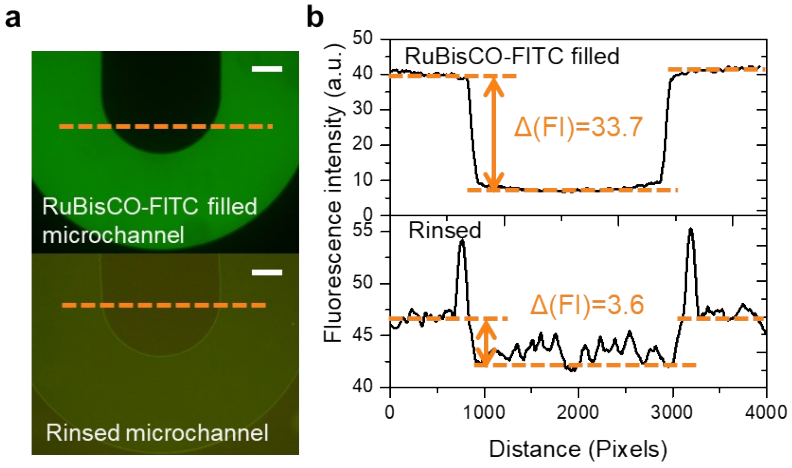

Figure S5. Fluorescence experiments for the confirmation of RuBisCO immobilization. (a) Fluorescence images of the RuBisCO-FITC filled microchannel (upper) and the rinsed microchannel (lower). (b) The corresponding fluorescence intensity profiles obtained along the observation lines. The scale bars are 500 μm.

Table S1. Measured kinetic parameters of the immobilized RuBisCO and the free RuBisCO

Enzyme immobilization type	V_{max} (mmol·min^{-1}·g^{-1} RuBisCO) [a)]	K_m [RuBP] (mM)
Physical immobilization	**0.008 ± 0.001**	**0.090 ± 0.028**
Chemical immobilization [b)]	0.070 ± 0.003	0.070 ± 0.012
Free in solution [c)]	0.169 ± 0.006	0.049 ± 0.008

[a)] The collected production solutions were 100 μL. RuBP concentrations were 0.025 – 2 mM for the RuBisCO immobilized by physical adsorption. The concentration of bicarbonate (HCO_3^-) in the reaction buffer was 66 mM. K_m and V_{max} values were the means ± s.d. of three independent experiments; [b), c)] The data were collected from our previous study using the same detection method.[1]

S5. ATR-FTIR spectra analysis

RuBisCO conformational change after immobilization was analyzed by ATR-FTIR. All the spectra of RuBisCO and RuBisCO immobilized on PDMS surface generally consisted of amide I and II bands at around 1700-1600 cm^{-1} and 1600-1500 cm^{-1}.[3] The spectra of the two bands were then normalized to 0 ~ 1 as shown in Figure S6a and S6b. Peak shifts were both observed for the amide II band (6 cm^{-1} shift in Figure S6a) and amide I band (2 cm^{-1} shift in Figure S6b) after RuBisCO was immobilized on PDMS. A strong change in the amide I band in the region 1620-1640 cm^{-1} was also noticed which could be corresponding to β-sheet.[4] To assess the secondary structure information on RuBisCO and RuBisCO immobilized on PDMS surface, the amide I bands of the two spectra after background subtracted were curve fitted with five protein secondary structural motifs: intermolecular β-sheets (1610-1627 cm^{-1}), β-sheets (1628-1642 cm^{-1}), random coils (1643-1650 cm^{-1}), α-helices/gin sidechains (1650-1659 cm^{-1}), and β-turns (1660-1699 cm^{-1}).[5-8] The fitted amide I bands were presented in Figure S6c and S6d, and the prediction of each secondary structure factions was summarized in Table S2. There was a significantly reduction in α-helices and an increase in intermolecular β-sheets and random coils when comparing the fractions of the RuBisCO immobilized on PDMS and that of RuBisCO solution, inferring the unfolding of RuBisCO after immobilization. The analysis of the ATR-FTIR spectra here clearly deduces the conformational change of RuBisCO after immobilization.

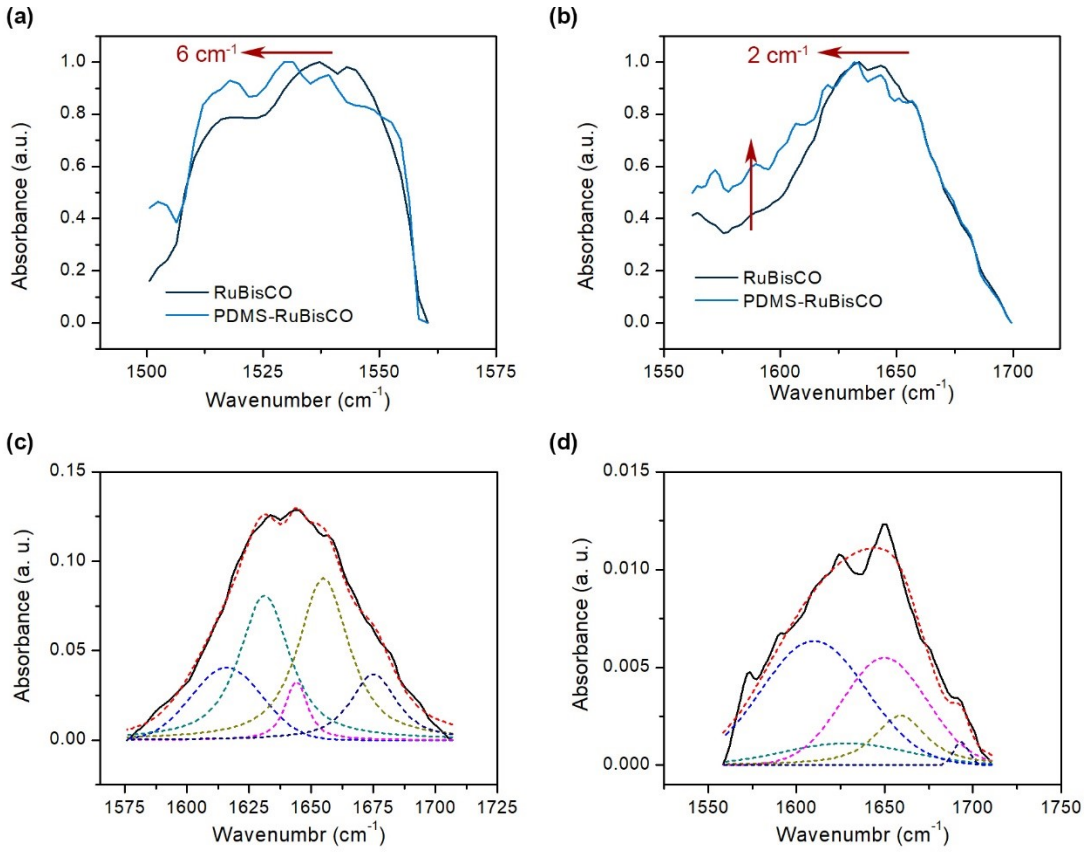

Figure S6. Analysis of the ATR-FTIR spectra of RuBisCO and RuBisCO adsorbed on PDMS. Normalized spectra for amide II band (a) and amide I band (b); Background subtracted amide I bands for secondary structural analysis curve fitting: (c) RuBisCO and (d) RuBisCO adsorbed on PDMS. The black lines represent the original experimental spectrum, and the red dashed lines represent the overall fitting lines. Component bands are given for intermolecular β-sheets (blue), β-sheets (dark cyan), random coils (magenta), α-helices/gin sidechains (dark yellow), and β-turns (navy).

Table S2. Secondary structure fractions (%) prediction of RuBisCO and RuBisCO immobilized on PDMS via curve fitting of the amide I bands of ATR-FTIR spectra

	intermolecular β-sheets	β-sheets	random coils	α-helices/gin sidechains	β-turns
RuBisCO	15.6	31.0	5.6	34.9	12.9
RuBisCO on PDMS	45.2	9.6	31.5	12.4	1.2

S6. Investigation of the conformational change of RuBisCO by circular dichroism spectrometer

In order to investigate the conformational change of RuBisCO after immobilization, RuBisCO solution and RuBisCO adsorbed on then PDMS thin films were prepared for circular dichroism (CD) measurements. All the CD spectra were collected by a JASCO J-1500 spectrophotometer at room temperature. The spectra of the solution samples were recorded over a wavelength range of 260–200 nm using a cuvette of 1-mm pathlength at a scan speed of 50 nm min^{-1} with the data integration time of 8s, a data pitch of 0.2 nm, and a bandwidth of 1 nm. Three accumulations were carried out per data point. The concentration of RuBisCO was about 0.2 mg mL^{-1} in the reaction buffer. Data were further processed for noise reduction, baseline subtraction, and signal averaging when needed. For the measurements of RuBisCO on film, about 200 μL of the RuBisCO in the reaction buffer (ca. 2 mg mL^{-1}) was cast onto a PDMS thin film for 4 h at room temperature. Then the PDMS thin film was washed by 200 μL of reaction buffer for 5 times. The washing buffer were collected for Bradford test after each washing step to check if there was any unbonded RuBisCO remained on the film. Then the CD spectra of the RuBisCO immobilized-PDMS thin film were recorded after the film was dried at room temperature. The parameters for recording the thin film were the same as the solution except for an unidentified film thickness (pathlength). The CD spectra of the PDMS thin film cast by the reaction buffer were also recorded as the control. All the data were presented as ellipticities (θ, mdeg) in Figure S6a.

As shown in the Figure S7a, the RuBisCO solution had the peak at ~220 nm (dark line).[9] But after RuBisCO was adsorbed on the PDMS slice, the negative peak of the spectrum was shifted to ~223 nm (blue line), while the spectrum of the reaction buffer on PDMS thin film showed no peaks (yellow line). The peak shift indicated the conformational change of RuBisCO after immobilization. The spectra were also analyzed by the deconvolution algorithms of CONTIN/LL[10, 11] to estimate the secondary structure fractions and were summarized in Table S3. It was noticed that after immobilization, the fraction of α-helices is greatly decreased, and the fractions of other structures were increased. The result was similar with the prediction by ATR-FTIR spectra, indicating the unfolding of RuBisCO after immobilization.

The Bradford tests were conducted to estimate the protein amount in the washing buffer after each washing step. As shown in the Figure S7b, protein could obviously be detected in the washing buffer collected from the first two steps of washing. The amount of the washed-off protein rapidly decreased with the increasing washing steps. Limited amount of protein was observed in the washing buffer after five times of washing, which help to induce that no unbonded RuBisCO were remained on the PDMS thin film for CD analysis. It could be concluded that the peak shift of the CD spectra was ascribed to the conformational change of the immobilized RuBisCO, other than the enzyme present in the solution.

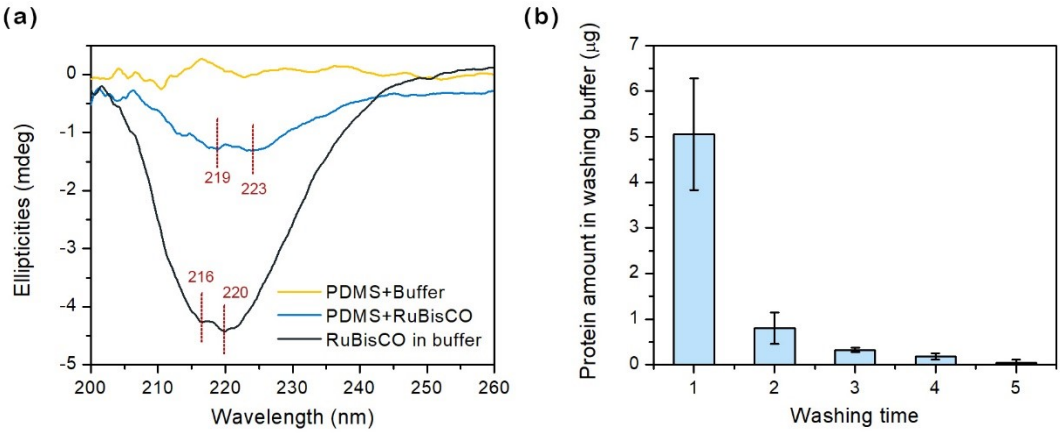

Figure S7. (a) Circular Dichroism (CD) spectra of RuBisCO in the reaction buffer (dark line), RuBisCO in the reaction buffer adsorbed on the PDMS slice (blue line) and reaction buffer on PDMS slice (yellow line). (b) The protein amount estimation in the washing buffer after each washing step determined by Bradford method.

Table S3. Secondary structure predictions of RuBisCO in reaction buffer and RuBisCO immobilized on PDMS film by CONTIN/LL[10, 11]

	%α*	$\%3_{10}$	%β	%T	%P	%U	%Total	NRMSD
RuBisCO	19.9	2.6	24.7	13.9	4.3	34.7	100.1	13.5
RuBisCO on PDMS	4.6	2.8	28.3	14.5	9.6	40.3	100.1	11.7

* α = alpha helix, 3_{10} = 3_{10} helix, β = beta sheet, T = turn, P = polyproline type II helix, U = unordered, NRMSD = normalized root mean square deviation.

Table S4. Performance comparison of the immobilized RuBisCO and the free RuBisCO

Enzyme immobilization type	3-PGA production rate (nmol·min^{-1})	Thermal stability [c]	Long-term thermal stability [d]	Reusability [e]	Recycling [f]
Physical immobilization	**0.145**	**57%**	**65%**	**40%**	**95%**
Chemical immobilization [a]	0.302	67%	75%	74%	-
Free in solution [b]	5.203	10%	47%	-	-

[a], [b] The data were collected from our previous study using the same detection method;[1] [c] Thermal stability was the remained relative activity after the incubation at 70 °C for 10 min; [d] Long-term thermal stability was the remained relative activity after the incubation at 50 °C for 60 min; [e] Reusability was the remained relative activity after 10 cycles of reuse at the flow rate of 7 μL min^{-1}; [f] Refreshing was the remained relative activity after 5 cycles of refreshing at the flow rate of 7 μL min^{-1}.

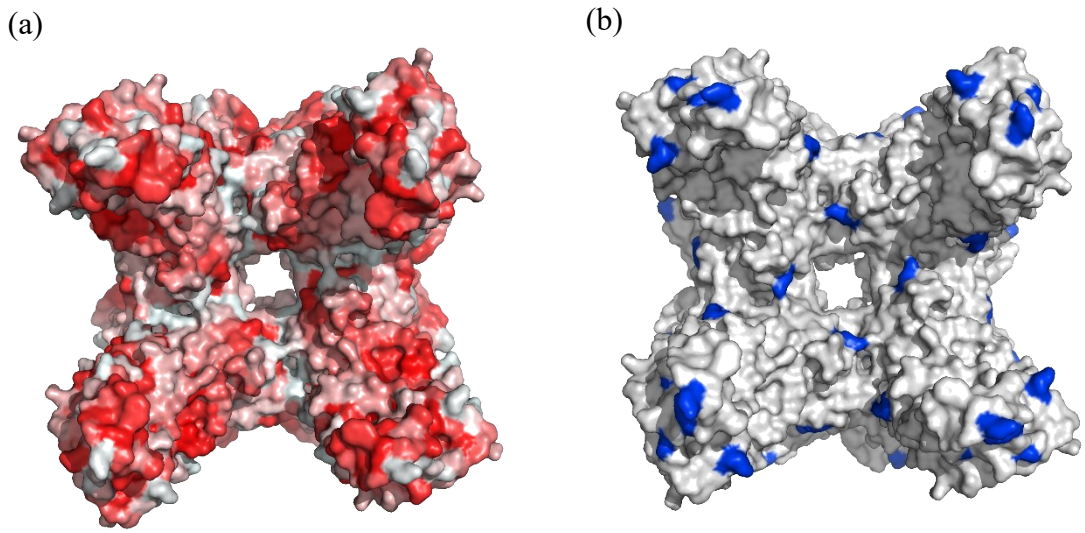

Figure S8. 3D structure images of RuBisCO (a) surface hydrophobicity (red: hydrophobic area; white: hydrophilic area) (b) possible covalent bonding sites (blue points: lysine) and of RuBisCO. Figures are prepared with PyMOL using the PDB co-ordinates 1RXO.

S7. Investigation of the activity loss of RI-PMRs after reusing

The reusability was evaluated at different flow rates (1 μL min^{-1}, 1.4 μL min^{-1}, 2.5 μL min^{-1}, 7 μL min^{-1} and 14 μL min^{-1}) to investigate the reason of activity loss after ten cycles of reuse. The washed-off protein amounts in the eluants were also estimated by injecting the reaction buffer at different flow rates and at the same time collecting 210 μL of the eluants from the outlet. As shown by the open blue circles in Figure S9a, the washed-off protein amount decreased with the increasing injection flow rates. The smaller the flow rate was, the less chance the enzyme had for detachment, but the longer the operation time of 10 cycles of reuse would be. The operation time was equal to the total volume collected from the outlet divided by the flow rate. Therefore, for the flow rate of 1 μL min^{-1}, the operation time for 10 cycles of reuse was as long as 210 min (Figure S9b). This implied that the immobilized enzyme in RI-PMRs was more likely to be detached after longer operation time. Notability, the percentages of the washed-off protein at different flow rates relative to the immobilized protein were as low as 0.2% ~ 0.5%. The enzyme being flushed-off might not be the main reason for the activity loss after reusing. It was the synergistic influence of enzyme deactivation and detachment after the reusing and the flushing. As shown by the solid blue squares in Figure S9a and S9b, the residual activity decreased with the decreasing flow rate. The immobilized enzyme lost its activity after long time reuses. It was inferred that the enzyme deactivation during the repeated uses may be the major reason for activity loss. However, for the chemically-immobilized RuBisCO microfluidic reactors, there was a maximum residual activity which appears at the flow rate of 1.4 μL min^{-1}.[1] Compared with the chemically-immobilized enzyme, the physically-immobilized enzyme was

more likely to be inactivated after long operation time. This might be because there is an intermediate linker that 'catches' the enzyme to maintain the enzyme structure after chemical immobilization, therefore reducing the loss of enzyme activity.[12] We proposed a model according to Hirsh's work[12] as shown in Figure S9c. For physical adsorption (left), RuBisCO would unfold and form into transient aggregate structures. After long time operation, the transient aggregate structure may rotate and expose the earlier adsorbed enzyme to solution. But for the chemical immobilization (right), RuBisCO is covalently bound to the surface, forming a monolayer. After long time operation, most of the enzyme structure can be retained due to the strong binding force.

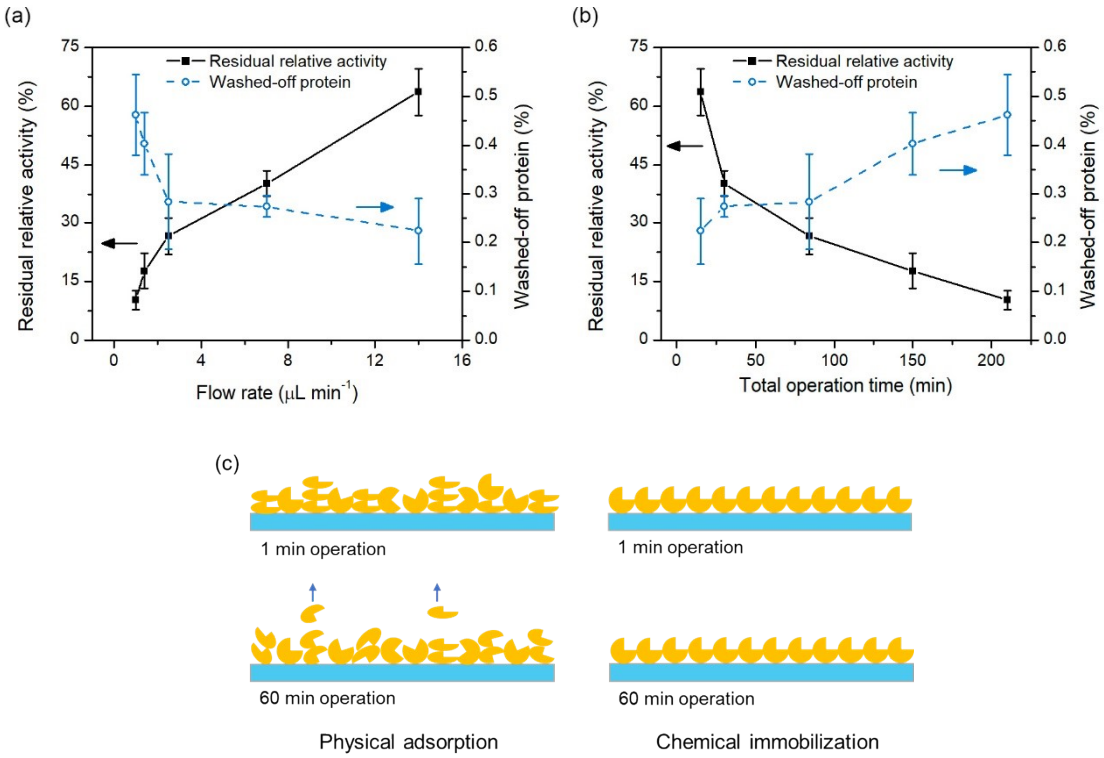

Figure S9. The residual relative activities for RI-PMRs (solid dark squares) after 10 cycles of reuse and the percentages of the washed-off protein amount relative to the protein loading amount for RI-PMRs (open blue circles) over different flow rates (a)

and the total operation time (b). (c) Schematic of the proposed model for RuBisCO immobilization on PDMS by physical adsorption (left) and chemical immobilization (right).

S8. Water contact angle analysis for the refreshing of the RI-PMRs

As shown in the water contact angle analysis in Figure S10, dark blue bar represents the water contact angle of the pristine PDMS, which is 103.8°. Light blue bars are the water contact angle results of PDMS after RuBisCO immobilization and grey bars are the results of PDMS when RuBisCO are desorbed by the acid buffer. After RuBisCO immobilization, the water contact angle of PDMS decreases from 103.8° to 69.1°. This hydrophilicity improvement results from the hydrophilic groups (carboxyl group) in RuBisCO. While after washing by the acid buffer, the PDMS recovers its hydrophobicity with the water contact angle of 96.2°. In the second cycle, the PDMS also becomes hydrophilic after RuBisCO immobilization and recovers to hydrophobicity after the desorption of RuBisCO (the water contact angles are 66.5° and 96.0°, respectively). These results reveal the effective desorption of RuBisCO by the acid buffer and the successful RuBisCO re-immobilization, which proves the feasibility of refreshing the PMRs. The insets are the photographs of the corresponding PDMS taken by CCD camera. Water contact angle results are calculated by the commercial software ImageJ. Error bars represent the standard deviations from three independent experiments.

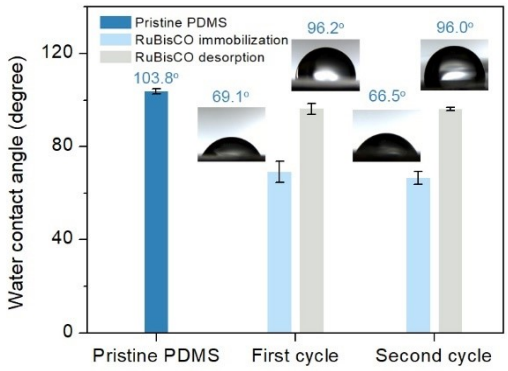

Figure S10. Water contact angle analysis for the refreshing of the RI-PMRs.

REFERENCES

1. Y. Zhu, Z. Huang, Q. Chen, Q. Wu, X. Huang, P.-K. So, L. Shao, Z. Yao, Y. Jia, Z. Li, W. Yu, Y. Yang, A. Jian, S. Sang, W. Zhang and X. Zhang, *Nat. Commun.*, 2019, **10**, 4049.
2. M. M. Bradford, *Anal. Biochem.*, 1976, **72**, 248-254.
3. A. Barth and C. Zscherp, *Q. Rev. Biophys.*, 2002, 35, 369-430.
4. D. Usoltsev, V. Sitnikova, A. Kajava and M. Uspenskaya, *Biomolecules*, 2019, 9, 359.
5. A. Sadat and I. J. Joye, *Appl. Sci.*, 2020, 10, 5918.
6. F. Liu, X. Li, A. Sheng, J. Shang, Z. Wang and J. Liu, *Environ. Sci. Technol.*, 2019, 53, 10157-10165.
7. Z. Xu and V. H. Grassian, *J. Phys. Chem. C*, 2017, 121, 21763-21771.
8. P. Roach, D. Farrar and C. C. Perry, *J. Am. Chem. Soc.*, 2005, 127, 8168-8173.
9. Y. Tomimatsu and J. W. Donovan, *Plant Physiol.*, 1981, **68**, 808-813.
10 B. R. Baker and R. L. Garrell, *Faraday Discuss.*, 2004, 126, 209-222.
11. S. W. Provencher and J. Gloeckner, *Biochemistry*, 1981, 20, 33-37.
12. S. L. Hirsh, M. M. M. Bilek, N. J. Nosworthy, A. Kondyurin, C. G. dos Remedios and D. R. McKenzie, *Langmuir*, 2010, **26**, 14380-14388.